

# Impact of Semi-annihilation of $\mathbb{Z}_3$ Symmetric Dark Matter with Radiative Neutrino Masses

Mayumi Aoki<sup>1\*</sup> and Takashi Toma<sup>2†</sup>

<sup>1</sup>*Institute for Theoretical Physics, Kanazawa University, Kanazawa 920-1192, Japan*

<sup>2</sup>*Institute for Particle Physics Phenomenology  
University of Durham, Durham DH1 3LE, United Kingdom*

## Abstract

We investigate a  $\mathbb{Z}_3$  symmetric model with two-loop radiative neutrino masses. Dark matter in the model is either a Dirac fermion or a complex scalar as a result of an unbroken  $\mathbb{Z}_3$  symmetry. In addition to standard annihilation processes, semi-annihilation of the dark matter contributes to the relic density. We study the effect of the semi-annihilation in the model and find that those contributions are important to obtain the observed relic density. The experimental signatures in dark matter searches are also discussed, where some of them are expected to be different from the signatures of dark matter in  $\mathbb{Z}_2$  symmetric models.

---

\*mayumi@hep.s.kanazawa-u.ac.jp

†takashi.toma@durham.ac.uk

# 1 Introduction

Non-zero small masses and mixings of the neutrinos have been confirmed by neutrino oscillation experiments such as solar, atmospheric, accelerator, and reactor neutrino experiments. All the data have been gathered together and the global fit of neutrino parameters has been done in ref. [1]. However the generation mechanism of neutrino masses is not known yet. It could be the canonical seesaw mechanism [2–4] in which the masses are derived with superheavy right-handed neutrinos, but verifying this experimentally is difficult.

On the other hand, the evidence for Dark Matter (DM) has been inferred from many observations, such as the rotation curves of spiral galaxies [5], the Cosmic Microwave Background [6] and the collision of the bullet cluster [7]. However, properties of the DM particle like its mass and interactions are not known. One of the most promising DM candidates is a Weakly Interacting Massive Particle (WIMP), which is thermally produced by decoupling from the thermal bath in the early universe. To reveal the nature of DM, various experiments including direct, indirect and collider searches are being operated.

Radiative seesaw models are one interesting possibility that address both of the issues above. Owing to the loop suppression, in these models the small neutrino masses are naturally obtained from TeV scale physics. In such models, the neutrino phenomenology often correlates with DM physics since a discrete symmetry like  $\mathbb{Z}_2$  parity forbids tree-level neutrino mass terms and also stabilizes the DM candidate. In addition to the representatives of well-known radiative models [8–12], many different models have been proposed and analyzed, see for example [13–35]. Although the  $\mathbb{Z}_2$  symmetry is introduced to stabilize the DM candidate in most of the models, other symmetries are possible. The second simplest symmetry is  $\mathbb{Z}_3$  and the properties have been studied [36–41]. In these models, semi-annihilation of DM such as  $\chi\chi \rightarrow \chi^\dagger X$  plays an important role in evaluating the DM relic density, where  $\chi$  is  $\mathbb{Z}_3$  charged DM and  $X$  is a Standard Model (SM) particle.<sup>1</sup>

In this paper, we consider a simple  $\mathbb{Z}_3$  symmetric model with the radiative neutrino masses at the two-loop level, which has been proposed in ref. [48]. The DM candidate in the model is either a Dirac fermion or a complex scalar. However, in ref. [48], it has been mentioned that both of them are unsuitable as DM candidate owing to the inconsistency with the experimental data of direct detection or Lepton Flavor Violation (LFV). Nevertheless, we will show that this conclusion changes when semi-annihilation processes are taken into account, which are specific properties of the  $\mathbb{Z}_3$  symmetric model. In the next section, the model is introduced and the two-loop induced neutrino masses are evaluated. Some experimental constraints are also discussed. In Section 3, the DM properties are investigated in detail for the Dirac fermion DM and the complex scalar DM, respectively. We discuss two cases for new Yukawa coupling with charged leptons  $y^\nu$ ; small  $y^\nu$  without

---

<sup>1</sup>Semi-annihilation of DM in models without a  $\mathbb{Z}_3$  symmetry have been discussed in the framework of vector boson DM [42–45], and in multi-component DM scenarios [41, 46, 47].

any specific flavor structure and large  $y^\nu$  with a specific flavor structure. In the calculation of the DM relic density, the semi-annihilation processes will give considerable effects. In particular for the Dirac DM, the severe constraints from LFV and the relic density of DM can be consistent due to the effects of semi-annihilations. Detectability of DM is also discussed from the view of direct, indirect and collider searches. The last two searches are especially interesting as they may infer the presence of semi-annihilation processes and therefore may distinguish between a  $\mathbb{Z}_2$  or  $\mathbb{Z}_3$  symmetry. Finally we summarize and conclude this work in Section 4.

## 2 The Model

The model considered here is quite simple. It was proposed and discussed briefly in ref. [48]. We introduce two Dirac fermions  $\psi_i$  ( $i = 1, 2$ ), and two scalar bosons  $\eta$  and  $\chi$  to the SM with  $\mathbb{Z}_3$  symmetry and lepton number as shown in Tab. 1.<sup>2</sup> The new scalars  $\eta$  and  $\chi$  are  $SU(2)_L$  doublet and singlet, respectively. Note that more than two Dirac fermions are required to generate at least two non-zero neutrino mass eigenvalues.<sup>3</sup> Here we add only two Dirac fermions for minimal particle content. The Lagrangian of the new particles is

$$\begin{aligned} \mathcal{L}_N = & \bar{\psi}_i (i\cancel{\partial} - m_i) \psi_i + (D_\mu \eta)^\dagger (D^\mu \eta) + \partial_\mu \chi^\dagger \partial^\mu \chi \\ & + \sum_{i,j} \left( y_{i\alpha}^\nu \eta \bar{\psi}_i P_L L_\alpha + \frac{y_{ij}^L}{2} \chi \bar{\psi}_i^c P_L \psi_j + \frac{y_{ij}^R}{2} \chi \bar{\psi}_i^c P_R \psi_j + \text{h.c.} \right), \end{aligned} \quad (1)$$

where  $i, j = 1, 2$ ,  $\alpha = e, \mu, \tau$  is the flavor index and  $L_\alpha = (\nu_\alpha, \ell_\alpha)^T$  is the left-handed lepton doublet. We can take  $\psi_i$  in the diagonal base without loss of generality. The gauge and  $\mathbb{Z}_3$  invariant renormalizable scalar potential  $\mathcal{V}$  is given by

$$\begin{aligned} \mathcal{V} = & \mu_\phi^2 \phi^\dagger \phi + \mu_\eta^2 \eta^\dagger \eta + \mu_\chi^2 \chi^\dagger \chi + \frac{\lambda_1}{4} (\phi^\dagger \phi)^2 + \frac{\lambda_2}{4} (\eta^\dagger \eta)^2 + \frac{\lambda_\chi}{4} (\chi^\dagger \chi)^2 \\ & + \lambda_3 (\phi^\dagger \phi) (\eta^\dagger \eta) + \lambda_4 (\phi^\dagger \eta) (\eta^\dagger \phi) + \lambda_{\phi\chi} (\phi^\dagger \phi) (\chi^\dagger \chi) + \lambda_{\eta\chi} (\eta^\dagger \eta) (\chi^\dagger \chi) \\ & + \left( \mu'_\chi (\phi^\dagger \eta) \chi^\dagger + \frac{\mu''_\chi}{3!} \chi^3 + \text{h.c.} \right), \end{aligned} \quad (2)$$

where  $\phi$  is the SM Higgs doublet. The second term in the third line softly breaks the lepton number conservation and is interpreted as the origin of neutrino masses. The phases of  $\mu'_\chi$  and  $\mu''_\chi$  are absorbed by the field redefinitions of  $\eta$  and  $\chi$ . This scalar potential is basically the same as that in the  $\mathbb{Z}_3$  DM model in ref. [37] except the term  $(\phi^\dagger \eta) \chi^2$ . This term is forbidden in our case due to the lepton number non-conservation. We assume that the new scalar bosons do not have vacuum expectation value:  $\langle \eta \rangle = \langle \chi \rangle = 0$ , otherwise the

<sup>2</sup>The  $\mathbb{Z}_3$  symmetry could be interpreted as a remnant symmetry of an extra  $U(1)$  symmetry as ref. [40].

<sup>3</sup>Several components of scalar  $\chi$  may be added to be consistent with neutrino masses instead of introducing multi-fermions [48].

	$\psi_i$	$\eta$	$\chi$
$SU(2)$	<b>1</b>	<b>2</b>	<b>1</b>
$U(1)_Y$	0	1/2	0
$\mathbb{Z}_3$	1	1	1
L number	1/3	-2/3	-2/3

Table 1: Charges of new particles where  $\psi_i$  ( $i = 1, 2$ ) are Dirac fermions,  $\eta$  and  $\chi$  are scalar bosons. For the other particles in the SM, zero charge of  $\mathbb{Z}_3$  is assigned.

$\mathbb{Z}_3$  symmetry which stabilizes the DM candidates breaks down. The sufficient conditions in order to get such a vacuum are given by [37],

$$\lambda_1, \lambda_2, \lambda_\chi, \lambda_{\phi\chi}, \lambda_{\eta\chi} > 0, \quad (3)$$

$$\lambda_3 + \lambda_4 > 0, \quad (4)$$

$$\frac{\mu_\chi'^2}{9\lambda_\chi} + \frac{\mu_\chi'^2}{(\lambda_3 + \lambda_4)} < \mu_\chi^2. \quad (5)$$

The parameters  $\mu_\phi^2$  and  $\lambda_1$  are determined by the vacuum expectation value and the mass of the SM Higgs boson,  $\langle\phi\rangle$  ( $\approx 174$  GeV) and  $m_h$ , as  $\mu_\phi^2 = -m_h^2/2 \approx -(89 \text{ GeV})^2$  and  $\lambda_1 = m_h^2/\langle\phi\rangle^2 \approx 0.5$ .

After the electroweak symmetry breaking, the neutral component of the SM Higgs boson  $\phi$  can be rewritten as  $\phi^0 = \langle\phi\rangle + h/\sqrt{2}$ , and the neutral scalars  $\eta^0$  and  $\chi$  mix with each other. A mass splitting between their real and imaginary parts does not occur so they remain as complex scalar particles. The mass matrix composed by  $\eta^0$  and  $\chi$  is given by

$$m_{\eta\chi}^2 \equiv \begin{pmatrix} m_{11}^2 & |m_{12}|^2 \\ |m_{12}|^2 & m_{22}^2 \end{pmatrix} = \begin{pmatrix} \mu_\eta^2 + (\lambda_3 + \lambda_4) \langle\phi\rangle^2 & \mu_\chi' \langle\phi\rangle \\ \mu_\chi' \langle\phi\rangle & \mu_\chi^2 + \lambda_{\phi\chi} \langle\phi\rangle^2 \end{pmatrix}. \quad (6)$$

Then the mass matrix is diagonalized by the rotation matrix

$$\begin{pmatrix} \eta^0 \\ \chi \end{pmatrix} = \begin{pmatrix} \cos \alpha & \sin \alpha \\ -\sin \alpha & \cos \alpha \end{pmatrix} \begin{pmatrix} \varphi_H \\ \varphi_L \end{pmatrix}, \quad (7)$$

with

$$\tan 2\alpha = \frac{2|m_{12}|^2}{m_{22}^2 - m_{11}^2} = \frac{2\mu_\chi' \langle\phi\rangle}{\mu_\chi^2 - \mu_\eta^2 + (\lambda_{\phi\chi} - \lambda_3 - \lambda_4) \langle\phi\rangle^2}, \quad (8)$$

where  $\varphi_H$  and  $\varphi_L$  are respectively the mass eigenstates with the masses  $m_H$  and  $m_L$  ( $m_H > m_L$ ).

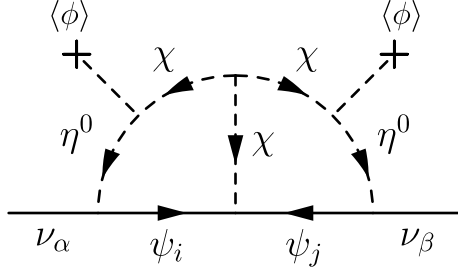


Figure 1: Diagram of neutrino mass generation at the two-loop level.

There are the following relationships among the parameters:

$$\mu'_\chi = -2 (m_H^2 - m_L^2) \frac{\cos \alpha \sin \alpha}{\langle \phi \rangle}, \quad (9)$$

$$\mu_\chi^2 = m_H^2 \sin^2 \alpha + m_L^2 \cos^2 \alpha - \lambda_{\phi\chi} \langle \phi \rangle^2, \quad (10)$$

$$m_{\eta^+}^2 = m_L^2 \sin^2 \alpha + m_H^2 \cos^2 \alpha - \lambda_4 \langle \phi \rangle^2, \quad (11)$$

$$\mu_\eta^2 = m_L^2 \sin^2 \alpha + m_H^2 \cos^2 \alpha - (\lambda_3 + \lambda_4) \langle \phi \rangle^2, \quad (12)$$

where  $m_{\eta^+}$  is the mass of the electromagnetic charged scalar  $\eta^+$ . Thus we can take  $m_L^2$ ,  $m_H^2$ ,  $\sin \alpha$ ,  $\lambda_2$ ,  $\lambda_3$ ,  $\lambda_4$ ,  $\lambda_\chi$ ,  $\lambda_{\phi\chi}$ ,  $\lambda_{\eta\chi}$ ,  $\mu''_\chi$  as the new independent parameter set in the scalar potential.

## 2.1 Neutrino Mass Matrix

In the model, the neutrino masses are induced at the two-loop level as shown in Fig. 1 [48]. The neutrino mass matrix is calculated as

$$(m_\nu)_{\alpha\beta} = \sum_{i,j} \frac{y_{i\alpha}^\nu y_{j\beta}^\nu \sin^2 2\alpha}{16(4\pi)^4} \mu''_\chi \left[ y_{ij}^L (I_L)_{ij} + y_{ij}^R (I_R)_{ij} \right], \quad (13)$$

where the loop function  $I_R$  is given below:

$$(I_R)_{ij} = \sin^2 \alpha (I_{Rij}^{HHH} - I_{Rij}^{HHL} - I_{Rij}^{LHH} + I_{Rij}^{LHL}) + \cos^2 \alpha (I_{Rij}^{HLL} - I_{Rij}^{HLL} - I_{Rij}^{LLH} + I_{Rij}^{LLL}), \quad (14)$$

and the function  $I_L$  is obtained by substituting  $R \rightarrow L$ . The functions  $I_{Lij}^{abc}$  and  $I_{Rij}^{abc}$  are given by

$$I_{Lij}^{abc} = \frac{m_j}{m_i} \int_0^1 dx dy dz \frac{\delta(x+y+z-1)}{y(1-y)} \left[ \frac{\xi_i^a \log \xi_i^a}{(1-\xi_i^a)(\xi_i^a - \xi_{ij}^{bc})} - \frac{\xi_{ij}^{bc} \log \xi_{ij}^{bc}}{(1-\xi_{ij}^{bc})(\xi_{ij}^{bc} - \xi_i^a)} \right], \quad (15)$$

$$I_{Rij}^{abc} = \int_0^1 dx dy dz \frac{\delta(x+y+z-1)}{1-y} \left[ \frac{\xi_i^{a2} \log \xi_i^a}{(1-\xi_i^a)(\xi_i^a - \xi_{ij}^{bc})} - \frac{\xi_{ij}^{bc2} \log \xi_{ij}^{bc}}{(1-\xi_{ij}^{bc})(\xi_{ij}^{bc} - \xi_i^a)} \right], \quad (16)$$

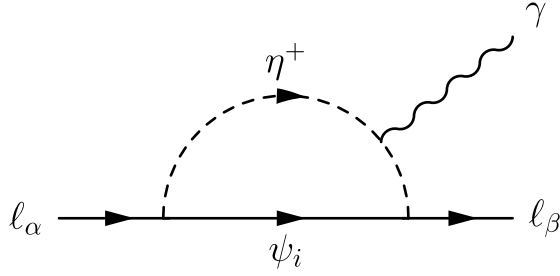


Figure 2: Feynman diagram of LFV process  $\ell_\alpha \rightarrow \ell_\beta \gamma$ .

with the parameters  $\xi_{ij}^a$  and  $\xi_{ij}^{bc}$  defined as

$$\xi_i^a \equiv \frac{m_a^2}{m_i^2}, \quad \xi_{ij}^{bc} \equiv \frac{xm_j^2 + ym_b^2 + zm_c^2}{y(1-y)m_i^2}, \quad a, b, c = H, L, \quad i, j = 1, 2. \quad (17)$$

As will be discussed later, the Yukawa coupling  $y^\nu$  should be naively  $y_{i\alpha}^\nu \lesssim 10^{-2}$  to avoid the constraint of LFV. If we take  $y_{i\alpha}^\nu \sim 0.01$ ,  $\sin \alpha \sim 0.1$  and  $(I_L)_{ij} \sim (I_R)_{ij} \sim 0.1$  for example, the required strength of the other couplings are estimated as  $\mu_\chi'' \sim 10$  GeV and  $y_{ij}^L \sim y_{ij}^R \sim 1$  in order to obtain the appropriate neutrino mass scale  $m_\nu \sim 0.1$  eV. The neutrino mass matrix should be diagonalized by the Pontecorvo-Maki-Nakagawa-Sakata (PMNS) matrix. Although we do not analyze the flavor structure here, it would be possible to obtain the observed values in the PMNS matrix because of many parameters in the formula of the neutrino mass matrix.

## 2.2 Experimental Constraints

The LFV process  $\ell_\alpha \rightarrow \ell_\beta \gamma$  is depicted in Fig. 2. The branching ratio for this process is

$$\text{Br}(\ell_\alpha \rightarrow \ell_\beta \gamma) = \frac{3\alpha_{\text{em}}}{64\pi G_F^2} \left| \sum_i \frac{y_{i\beta}^{\nu*} y_{i\alpha}^\nu}{m_i^2} F_i^{\text{loop}} \right|^2 \text{Br}(\ell_\alpha \rightarrow \ell_\beta \nu_\alpha \bar{\nu}_\beta), \quad (18)$$

where  $G_F$  is Fermi constant and the loop function  $F_i^{\text{loop}}$  is given by

$$F_i^{\text{loop}} = \cos^4 \alpha F_2'(\xi_i^H, \xi_i^H) + 2 \cos^2 \alpha \sin^2 \alpha F_2'(\xi_i^H, \xi_i^L) + \sin^4 \alpha F_2'(\xi_i^L, \xi_i^L), \quad (19)$$

and  $F_2'(x, y)$  is defined as

$$F_2'(x, y) = \frac{f(x) - f(y)}{x - y} \quad \text{with} \quad f(x) = -\frac{5 - 27x + 27x^2 - 5x^3 + 6x^2(x - 3) \log x}{36(1 - x)^3}. \quad (20)$$

In particular when we take the limit of  $y \rightarrow x$ , the function  $x^{-1} F_2'(x^{-1}, x^{-1})$  corresponds to the function  $F_2(x)$  defined in ref. [49]. The most stringent constraint comes from the  $\mu \rightarrow e \gamma$  whose upper bound of the branching ratio is  $\text{Br}(\mu \rightarrow e \gamma) \leq 5.7 \times 10^{-13}$  [50], and

it will be improved to  $6 \times 10^{-14}$  in future [51]. Choosing  $F_i^{\text{loop}} \sim 0.1$  with  $\xi_i^H \sim \xi_i^L \sim 1$ , the requirement for the constraint is roughly written as

$$|y_{ie}^{\nu*} y_{i\mu}^{\nu}| \left( \frac{m_i}{100 \text{ GeV}} \right)^{-2} \lesssim 5 \times 10^{-5}. \quad (21)$$

Hence for example when  $m_i = 200 \text{ GeV}$ , the Yukawa coupling is restricted to  $y_{i\alpha}^{\nu} \lesssim 10^{-2}$  if we do not assume a certain flavor structure. Another solution to escape the LFV constraint is to assume a specific flavor structure or a diagonal form for the Yukawa matrix.<sup>4</sup> In this case,  $y^{\nu}$  does not contribute to LFV and we can take  $\mathcal{O}(1)$  coupling in some elements of  $y^{\nu}$ . Then the neutrino mixing is derived from the other Yukawa couplings  $y^L$  and  $y^R$ . As we will discuss later, this solution is interesting because larger  $\mathbb{Z}_3$  DM may be more easily detected. The constraint from another LFV process  $\mu \rightarrow 3e$  might be taken into account depending on the parameter space. This process would be enhanced compared to the  $\mu \rightarrow e\gamma$  process by the box diagrams when the Yukawa coupling  $y^{\nu}$  is large enough, as has been discussed in ref. [52, 53].

The mass difference between the charged scalar  $\eta^+$  and the neutral scalars  $\varphi_{H,L}$  is constrained by ElectroWeak Precision Tests (EWPT). Basically, the calculation for our model is the same with the inert doublet model. The new contribution to T-parameter,  $\Delta T$  is calculated as [54]

$$\alpha_{\text{em}} \Delta T = \frac{1}{2(4\pi)^2 \langle \phi \rangle^2} \left[ \cos^2 \alpha F(m_{\eta^+}^2, m_H^2) + \sin^2 \alpha F(m_{\eta^+}^2, m_L^2) \right], \quad (22)$$

where the function  $F(x, y)$  is

$$F(x, y) = \frac{x+y}{2} - \frac{xy}{x-y} \log \left( \frac{x}{y} \right). \quad (23)$$

From these formulae, the constraint on the mass difference between  $\eta^+$  and  $\varphi_{H,L}$  is approximately given by [54, 55]

$$\cos^2 \alpha (m_{\eta^+} - m_H)^2 + \sin^2 \alpha (m_{\eta^+} - m_L)^2 \lesssim (140 \text{ GeV})^2. \quad (24)$$

### 3 Dark Matter Properties

There are two DM candidates in this model, the lightest Dirac fermion  $\psi_1$  or the lightest mass eigenstate of the scalar boson  $\varphi_L$ . Since the decay process  $\psi_1 \rightarrow \varphi_L \nu_\alpha$  or  $\varphi_L \rightarrow \psi_1 \nu_\alpha$  is possible in the model depending on the mass spectrum, either of them can be DM. We rename hereafter the Dirac fermion DM as  $\psi$  with the mass  $m_\psi$  and the scalar one as  $\varphi$  with the mass  $m_\varphi$ , and discuss the DM properties in the following.

---

<sup>4</sup>One may confuse the meaning of “diagonal” here since the Yukawa matrix  $y^{\nu}$  is not a square matrix. In our case, “diagonal” means at least  $y_{1\mu}^{\nu} = y_{2e}^{\nu} = y_{1\tau}^{\nu} = y_{2\tau}^{\nu} = 0$ .

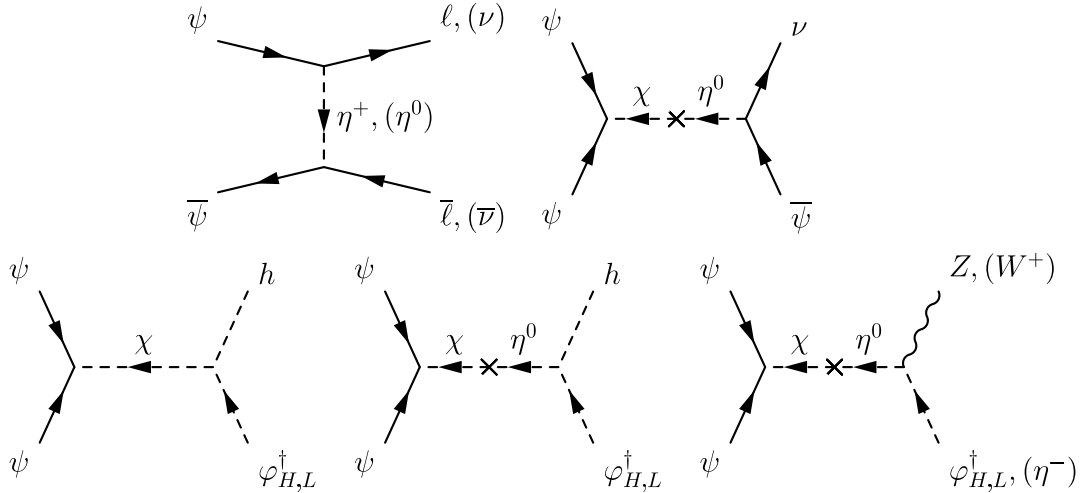


Figure 3: Diagrams of (semi-)annihilation processes of Dirac DM  $\psi$ . The t-channel diagram of the top right one also exists.

### 3.1 Dirac Fermion Dark Matter

For the Dirac fermion DM  $\psi$ , in addition to the annihilation channels, we have some semi-annihilation channels like  $\psi\psi \rightarrow \nu\bar{\psi}, h\varphi^\dagger, Z\varphi^\dagger$  as shown in Fig. 3. The evolution of the number density of Dirac DM is determined by the Boltzmann equation:

$$\frac{dn_\psi}{dt} + 3Hn_\psi = -\langle\sigma v_{\psi\bar{\psi}}\rangle (n_\psi^2 - n_\psi^{\text{eq}2}) - \frac{1}{2}\langle\sigma v_{\psi\psi}\rangle (n_\psi^2 - n_\psi n_\psi^{\text{eq}}), \quad (25)$$

where the number densities of  $\psi$  and  $\bar{\psi}$  are assumed to be the same  $n_\psi = n_{\bar{\psi}}$ . This assumption is valid as long as CP invariance is considered. The first term in the right-hand side of Eq. (25) implies the standard annihilation processes and the second term corresponds to the semi-annihilation processes. The factor 1/2 in the second term comes from taking into account the processes  $\psi\psi \rightarrow X\bar{\psi}$  and  $\bar{\psi}\bar{\psi} \rightarrow \bar{X}\psi$  both where  $X$  is any set of the SM particles. The contribution of the decay processes such as  $\varphi_L \rightarrow \psi\nu_\alpha$  is negligible unless the decaying particle has an extremely long lifetime, considered since the DM is still in the thermal bath when the decay process decouples. We construct our own model with LanHEP [56]<sup>5</sup>, and then micrOMEGAs is used to solve the Boltzmann equation numerically [58]. In general, off-shell annihilation processes such as  $\psi\psi \rightarrow Z^*\varphi_{H,L}^\dagger$  are also included in our numerical analysis.

If any semi-annihilation channels are not significant, only annihilation processes  $\psi\bar{\psi} \rightarrow \bar{\ell}\bar{\ell}, \nu\bar{\nu}$  affect the thermal relic density of the Dirac DM. The cross section is proportional to  $|y_{1\alpha}^{\nu*}y_{1\beta}^\nu|^2$ , and the required order of the Yukawa coupling is roughly  $y_{1\alpha}^\nu \sim \mathcal{O}(0.1 - 1)$  to be compatible with the observed relic density  $\Omega h^2 \approx 0.12$  [6]. However the Yukawa coupling is severely constrained by the LFV processes as have discussed in the previous section.

<sup>5</sup>Feynrules is useful to construct a model [57].



	$\lambda_{\phi\chi}$	$m_L$ [GeV]	$m_H$ [GeV]	$y^\nu$	$y^L, y^R$
BM-F1	0.1	400	500	$\begin{pmatrix} 0.01 & 0.01 & 0.01 \\ 0.01 & 0.01 & 0.01 \end{pmatrix}$	$\mathcal{O}(1)$
BM-F2	0.1	400	400		
BM-F3	1.0	400	500		
BM-F4	1.0	400	400		
BM-F1'	0.1	400	500	$\begin{pmatrix} 0.5 & 0 & 0 \\ 0 & 0.5 & 0 \end{pmatrix}$	$\mathcal{O}(0.1)$
BM-F2'	0.1	400	400		
BM-F3'	1.0	400	500		
BM-F4'	1.0	400	400		

Table 2: Benchmark parameter sets for Fig. 4 and 5. The other parameters are fixed to  $\lambda_2 = \lambda_\chi = \lambda_{\eta\chi} = 0.1$ ,  $\lambda_3 = \lambda_4 = 0.5$  and  $m_2 = 1$  TeV. The parameter  $\mu_\chi'' \sin^2 \alpha$  is fixed to 100 MeV for the upper four sets, and 1 MeV for the lower four sets. The mass of  $\eta^+$  is determined by Eq. (11).

One needs roughly  $y_{i\alpha}^\nu \lesssim 0.01$  to avoid the  $\mu \rightarrow e\gamma$  constraint. Thus it seems to be difficult to satisfy the correct thermal relic density only with the annihilation channel. The effect of semi-annihilation is important to give consistency to both the DM relic density and LFV as will be discussed in Sec. 3.1.1. Another solution is the consideration of mass degeneration with the other new particles [59, 60], then the relic density is reduced by co-annihilation with the degenerated particles. In particular co-annihilation with  $\eta$  gives a large contribution to the effective cross section since it has gauge interactions.

Meanwhile, taking a larger Yukawa coupling  $y^\nu$  can be possible if a special flavor texture to suppress the LFV processes is assumed [59, 60]. This possibility will be discussed in Sec. 3.1.2.

### 3.1.1 Small Yukawa Coupling

The DM mass dependence of the relic density is illustrated in Fig. 4 for the small Yukawa couplings. The masses of the  $\mathbb{Z}_3$  charged scalars and the other parameters in the model are fixed to the benchmark sets as shown in Tab. 2. For the parameter sets of BM-F1 and BM-F3, the masses of scalars are set as  $m_L = 400$  GeV and  $m_H = 500$  GeV, and the charged scalar mass is fixed by Eq. (11). There are two damped regions, around 200 GeV and 250 GeV in the left upper and lower panels of Fig. 4. The first damped region results from the resonance of  $\varphi_L$  in the semi-annihilation processes  $\psi\psi \rightarrow \varphi_L \rightarrow \nu\bar{\psi}$ , while the second one corresponds to the  $\varphi_H$  resonance in mainly  $\psi\psi \rightarrow \varphi_H \rightarrow W^+\eta^-, Z\varphi_L^\dagger$ . Thus one can satisfy the correct relic density of DM without any contradictions thanks to the resonances of the semi-annihilation channels. The co-annihilation with  $\varphi_L$  is effective around 400 GeV for BM-F1 and BM-F3. When a large  $\lambda_{\phi\chi}$  is taken as BM-F3, the semi-annihilation process  $\psi\psi \rightarrow \varphi_L \rightarrow h\varphi_L^\dagger$  is enhanced even if the mixing  $\sin \alpha$  is zero. This

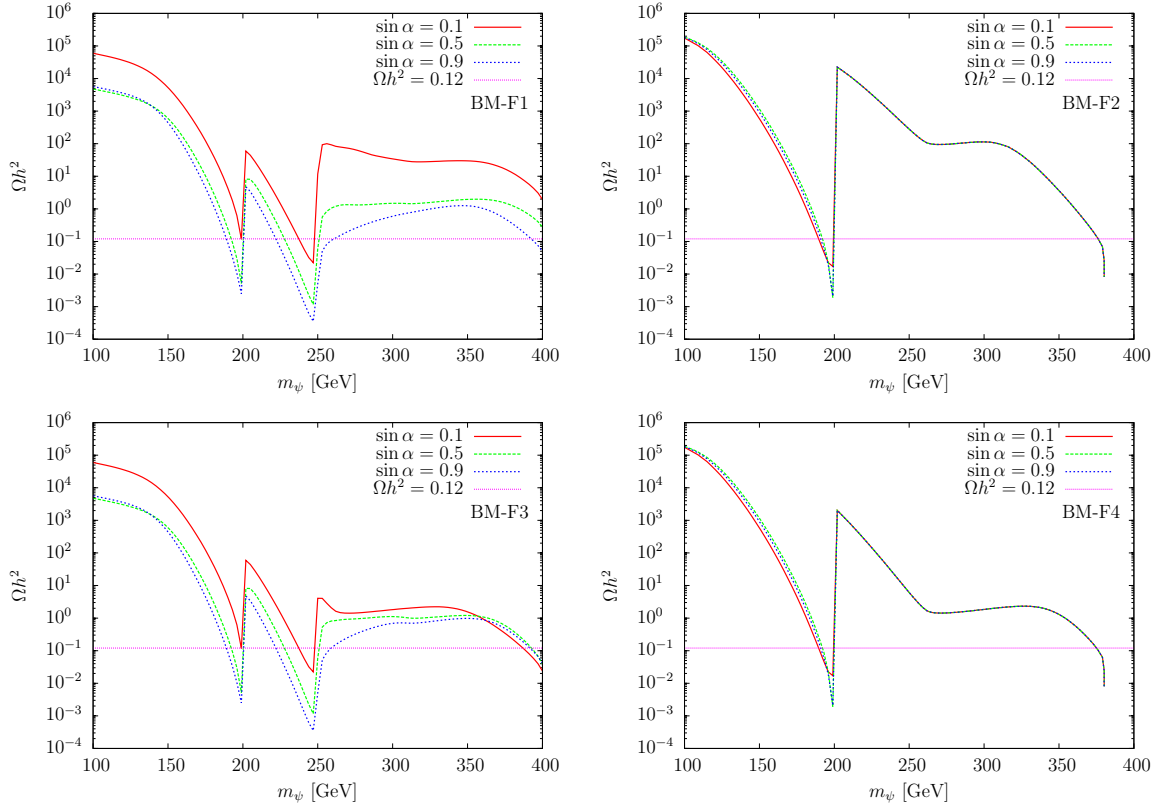


Figure 4: DM mass dependence of the relic density. The upper panels are for BM-F1 and BM-F2, and the lower panels are for BM-F3 and BM-F4.

process starts to be effective around  $m_\psi = (m_h + m_{\varphi_L})/2 \approx 260$  GeV. As found in the lower left panel in Fig. 4, the relic abundance of DM is much reduced in the region of  $m_\psi \gtrsim 260$  GeV for large  $\lambda_{\phi\chi}$ . The effect of  $\lambda_{\phi\chi}$  is significant in particular for small mixing angle.

In the right panels for BM-F2 and BM-F4, the masses of  $\varphi_L$  and  $\varphi_H$  are both fixed to 400 GeV. The behavior is quite different from the former case. The sharp damping around 200 GeV comes from the dominant semi-annihilation  $\psi\psi \rightarrow \varphi_{H,L} \rightarrow \nu\bar{\psi}$ , but the second damped region disappears. Thus the observed relic density is achieved only at the damped and the co-annihilation region with  $\varphi_{H,L}$ . Another difference from the left panels is that the dependence of the mixing angle is extremely small. This is because when the masses are degenerated, the scalar couplings in the potential have almost no dependence on the mixing angle as one can see from Eq. (9)–(12). The maximum DM mass is bounded by the charged scalar mass  $m_{\eta^+} \approx 380$  GeV.

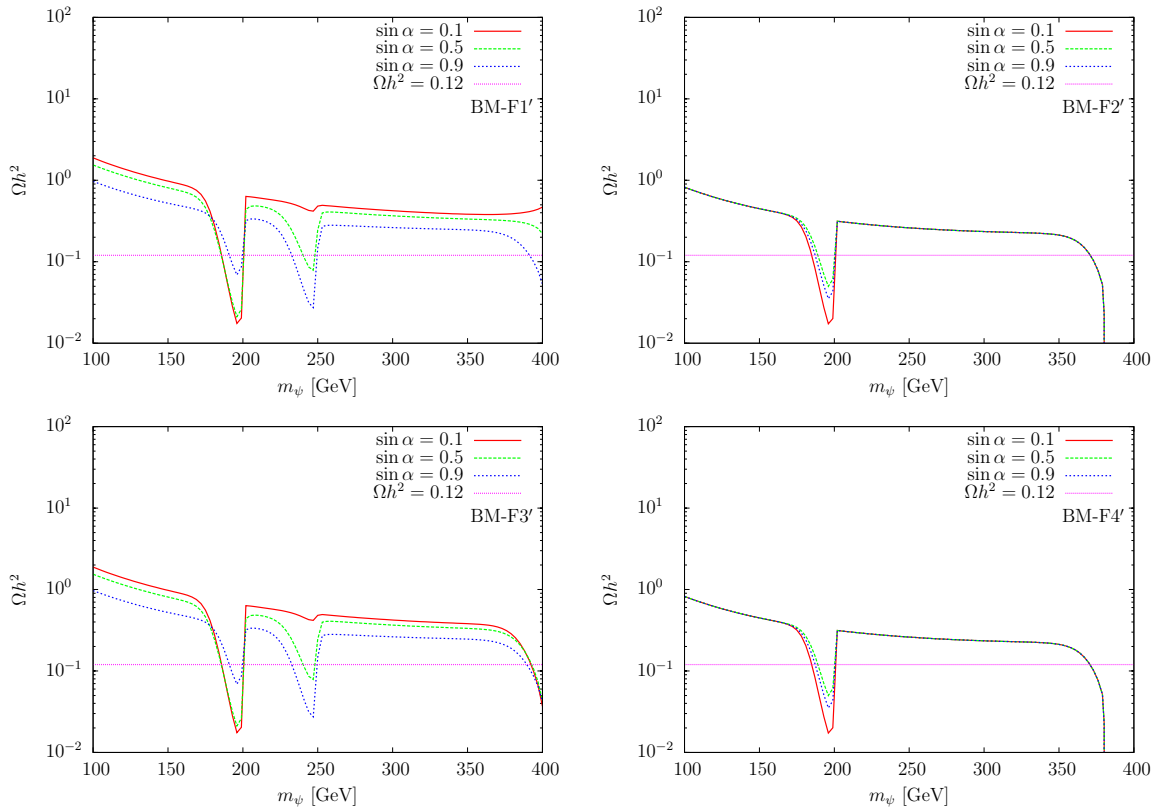


Figure 5: DM mass dependence of the relic density for some parameter sets. The upper panels correspond to BM-F1' and BM-F2', and the lower panels are for BM-F3' and BM-F4'. Details of the parameter sets are in Tab. 2.

### 3.1.2 Large Yukawa Coupling

Suppressing the LFV while having large Yukawa couplings is allowed by choosing a specific flavor structure for the Yukawa matrix  $y^\nu$ . This case is quite interesting from view of the detectability of the Dirac DM as we will discuss later. In Fig. 5, we show the DM mass dependence of the relic density for the benchmark sets BM-F1', BM-F2', BM-F3' and BM-F4'. These parameter sets are the same as in Tab. 2 for BM-F1, BM-F2, BM-F3 and BM-F4 respectively, but the values of the parameters  $y^\nu$ ,  $y^L$ ,  $y^R$  and  $\mu''_\chi$  are different. The Yukawa coupling  $y^\nu$  is fixed to  $y''_{1e} = y''_{2\mu} = 0.5$  and  $y''_{1\mu} = y''_{2e} = 0$  to suppress the  $\mu \rightarrow e\gamma$  process. The other components of  $y^\nu$  are also fixed adequately. The Yukawa couplings  $y^L$  and  $y^R$  are taken as  $y^L \sim y^R \sim \mathcal{O}(0.1)$ . Then the known neutrino mass scale can be obtained by adjusting the cubic coupling  $\mu''_\chi$  to satisfy  $\mu''_\chi \sin^2 \alpha \sim 1$  MeV from Eq. (13).

Since the Yukawa coupling  $y^\nu$  is large, the standard annihilation channels  $\psi\bar{\psi} \rightarrow \ell\bar{\ell}, \nu\bar{\nu}$  give some contribution to the total annihilation cross section throughout Fig. 5. In these parameter sets, the cross sections of the annihilation and semi-annihilation processes can

be comparable, and the dependence of the scalar coupling  $\lambda_{\phi\chi}$  becomes relatively smaller than the case of small Yukawa coupling. This can be seen in the figure. The variation of the relic density in terms of the DM mass for the large Yukawa coupling is much milder than that for the small Yukawa coupling, as can be seen from Fig. 4 and Fig. 5.

## 3.2 Detectability of Dirac Fermion Dark Matter

### 3.2.1 Direct Search

The Dirac DM  $\psi$  can interact with quarks at one-loop level via photon and  $Z$  exchanges as depicted in Fig. 6. Since the one-loop interactions are described by the Yukawa coupling  $y^\nu$ ,  $y^L$  and  $y^R$ , the case of large Yukawa coupling discussed above should especially be compared with experimental limits. When the Yukawa couplings are small, the scattering cross section is small and will not be detected in the near future. The following relevant interactions are obtained through the one-loop diagram,

$$\begin{aligned} \mathcal{L}_{\text{eff}} = & a_\psi \bar{\psi} \gamma^\mu \psi \partial^\nu F_{\mu\nu} + \left( \frac{\mu_\psi}{2} \right) \bar{\psi} \sigma^{\mu\nu} \psi F_{\mu\nu} + c_\psi A_\mu \bar{\psi} \gamma^\mu \psi \\ & + Z_\mu \bar{\psi} (V_\psi \gamma^\mu + A_\psi \gamma^\mu \gamma_5) \psi, \end{aligned} \quad (26)$$

where  $F_{\mu\nu}$  is the electromagnetic field strength and the couplings  $a_\psi$ ,  $\mu_\psi$ ,  $c_\psi$  are given by [60]

$$a_\psi = - \sum_\alpha \frac{|y_{1\alpha}^\nu|^2 e}{4(4\pi)^2 m_{\eta^+}^2} I_a \left( \frac{m_\psi^2}{m_{\eta^+}^2}, \frac{m_\alpha^2}{m_{\eta^+}^2} \right), \quad (27)$$

$$\mu_\psi = - \sum_\alpha \frac{|y_{1\alpha}^\nu|^2 e}{4(4\pi)^2 m_{\eta^+}^2} 2m_\psi I_m \left( \frac{m_\psi^2}{m_{\eta^+}^2}, \frac{m_\alpha^2}{m_{\eta^+}^2} \right), \quad (28)$$

$$c_\psi = + \sum_\alpha \frac{|y_{1\alpha}^\nu|^2 e}{4(4\pi)^2 m_{\eta^+}^2} q^2 I_c \left( \frac{m_\psi^2}{m_{\eta^+}^2}, \frac{m_\alpha^2}{m_{\eta^+}^2} \right), \quad (29)$$

where  $q^2$  is the transfer momentum to the gauge boson. The loop functions  $I_a(x, y)$ ,  $I_m(x, y)$  and  $I_c(x, y)$  are given in ref. [60]. The factor  $\log y$  is included in the loop function  $I_a(x, y)$ , and it leads to some enhancement of the interaction. The interactions with  $Z$  boson are calculated as

$$\begin{aligned} V_\psi = & - \frac{g_2 \sin^2 2\alpha}{32(4\pi)^2 \cos \theta_W} \sum_i \left( |y_{i1}^L|^2 + |y_{i1}^R|^2 \right) \sum_{a,b=H,L} \text{sgn}(a, b) I_{V1}(\xi^i, \xi^a, \xi^b) \\ & - \frac{g_2 \sin^2 2\alpha}{32(4\pi)^2 \cos \theta_W} \sum_i \left( y_{i1}^L y_{i1}^{R*} + y_{i1}^{L*} y_{i1}^R \right) \sum_{a,b=H,L} \text{sgn}(a, b) I_{V2}(\xi^i, \xi^a, \xi^b), \end{aligned} \quad (30)$$

$$A_\psi = + \frac{g_2 \sin^2 2\alpha}{32(4\pi)^2 \cos \theta_W} \sum_i \left( |y_{i1}^L|^2 - |y_{i1}^R|^2 \right) \sum_{a,b=H,L} \text{sgn}(a, b) I_A(\xi^i, \xi^a, \xi^b), \quad (31)$$

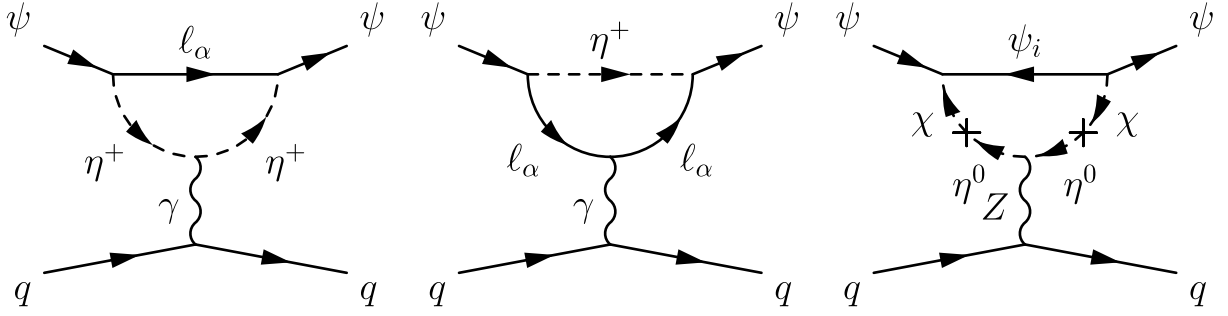


Figure 6: Diagram of primary contributions to spin independent and spin dependent cross section for Dirac DM  $\psi$ .

with

$$\xi^i \equiv \frac{m_i^2}{m_\psi^2}, \quad \xi^L \equiv \frac{m_L^2}{m_\psi^2}, \quad \xi^H \equiv \frac{m_H^2}{m_\psi^2}. \quad (32)$$

The coefficient  $g_2$  is the  $SU(2)_L$  gauge coupling constant and  $\sin \theta_W$  is the Weinberg angle. The sign function  $\text{sgn}(a, b)$  is defined as  $\text{sgn}(H, H) = \text{sgn}(L, L) = 1$  and  $\text{sgn}(H, L) = \text{sgn}(L, H) = -1$ , and the loop functions  $I_{V1}$ ,  $I_{V2}$  and  $I_A$  are

$$I_{V1}(x, y, z) = \int_0^1 \frac{1 - 2u + 2u^2}{2(y - z)} \log \left( \frac{ux + (1 - u)(y - u)}{ux + (1 - u)(z - u)} \right) du, \quad (33)$$

$$I_{V2}(x, y, z) = \int_0^1 \frac{\sqrt{x}}{y - z} \log \left( \frac{ux + (1 - u)(y - u)}{ux + (1 - u)(z - u)} \right) du, \quad (34)$$

$$I_A(x, y, z) = \int_0^1 \frac{1}{2(y - z)} \log \left( \frac{ux + (1 - u)(y - u)}{ux + (1 - u)(z - u)} \right) du. \quad (35)$$

The couplings  $V_\psi$  and  $A_\psi$  vanish when the  $\mathbb{Z}_3$  charged bosons  $\varphi_L$  and  $\varphi_H$  are completely degenerate. Since these interactions are proportional to  $\sin^2 2\alpha$ , one can expect that a moderate cross section is derived when the mixing angle is large.

In these effective interactions, the couplings  $a_\psi$ ,  $c_\psi$  and  $V_\psi$  contribute to the four Fermi vector interaction with quarks:  $b_\psi \bar{q} \gamma_\mu q \bar{\psi} \gamma^\mu \psi$ . The contribution via  $Z$  boson is small compared to the photon contribution if the Yukawa couplings  $y^\nu$  and  $y^{L,R}$  are of the same order. Neglecting the  $Z$  boson contribution, the four Fermi interaction  $b_\psi$  is given by  $b_\psi = (a_\psi + c_\psi/q^2)e$ , namely

$$b_\psi = - \sum_\alpha \frac{|y_{1\alpha}^\nu|^2 e^2}{4(4\pi)^2 m_{\eta^+}^2} I_b \left( \frac{m_\psi^2}{m_{\eta^+}^2}, \frac{m_\alpha^2}{m_{\eta^+}^2} \right), \quad (36)$$

where  $I_b(x, y) = I_a(x, y) - I_c(x, y)$ . The spin independent elastic cross section with nucleus at zero transfer momentum via the vector interaction is calculated as

$$\sigma_{\text{SI}} = Z^2 \frac{b_\psi^2}{\pi} \frac{m_\psi^2 m_A^2}{(m_\psi + m_A)^2}, \quad (37)$$

where  $Z$  and  $m_A$  are atomic number and mass of nucleus. For example, the elastic cross section to scatter with a proton with the parametrization BM-F1' is estimated as  $\sigma_{\text{SI}} \sim 10^{-45} \text{ cm}^2$ , which is slightly below the upper bound from LUX for  $m_\psi \gtrsim 100 \text{ GeV}$  [61]. Thus it would be detected by near-future direct detection experiments such XENON1T [62]. In fact there is another contribution to the spin independent cross section via the magnetic moment of DM  $\mu_\psi$ . However this contribution diverges at zero recoil energy and we cannot define adequately the total cross section at zero momentum transfer. Moreover this contribution is sub-dominant because of the enhancement factor  $\log y$  of  $I_a(x, y)$  in the effective coupling  $a_\psi$ , as already pointed out above. Thus we do not include this contribution in our discussion. If more careful treatment is required, this contribution should be taken into account.

The couplings  $\mu_\psi$  and  $A_\psi$  contribute to the spin dependent cross section. As with the the spin independent cross section, the effective interaction via a  $Z$  boson is sub-dominant. Thus the spin dependent cross section at zero momentum transfer is simply given by

$$\sigma_{\text{SD}} = \frac{2\mu_\psi^2 \mu_A^2}{\pi} \frac{m_\psi^2 m_A^2}{(m_\psi + m_A)^2} \left( \frac{J_A + 1}{3J_A} \right), \quad (38)$$

where  $\mu_A$  and  $J_A$  are the magnetic moment and the spin of nucleus, respectively. For the large Yukawa benchmark parameter sets, the order of the cross section with a proton is roughly estimated as  $\sigma_{\text{SD}} \sim 10^{-45} \text{ cm}^2$ . The present strongest upper bound on the spin dependent cross section is given as  $\sigma_{\text{SD}} \lesssim 10^{-39} \text{ cm}^2$  by COUPP [63] and SIMPLE [64], which is too weak to constrain the model.

In addition, there are further more severe constraints on the spin dependent cross section from the search for neutrinos from the Sun by IceCube [65]. These limits hold when the capture rate and the annihilation rate of DM in the Sun are in equilibrium. As a result, the capture rate which depends on both the spin independent and dependent cross section is constrained, depending on annihilation mode of DM.

### 3.2.2 Indirect Search

In general, semi-annihilation processes are present when we consider a larger symmetry than  $\mathbb{Z}_2$  for stabilizing DM, such as a  $\mathbb{Z}_3$  symmetry. A characteristic implication of semi-annihilation may be observed in indirect searches of DM [36, 38, 47]. In our case, we have two channels for generating monochromatic neutrinos,  $\psi\bar{\psi} \rightarrow \nu\bar{\nu}$  and  $\psi\psi \rightarrow \nu\bar{\psi}$ , whose energies are determined kinematically as  $E_\nu = m_\psi$  and  $3m_\psi/4$  respectively. Thus a double peak may be detected in the neutrino flux from the galaxy or the Sun as a signature of the model with the semi-annihilation of DM [36]. A large Yukawa coupling  $y'$  with a special flavor structure is necessary to see the signal of the double peak.

For the large Yukawa parameter sets, the standard annihilation  $\psi\bar{\psi} \rightarrow \nu\bar{\nu}$  and the semi-annihilation  $\psi\psi \rightarrow \nu\bar{\psi}$  can be the main channels and comparable each other in some parameter regions, as shown in the previous section. The present upper bound for the annihilation cross section into neutrinos from the galactic center is  $\langle\sigma v\rangle_{\nu\bar{\nu}} \lesssim 10^{-22} \text{ cm}^3/\text{s}$  [67],

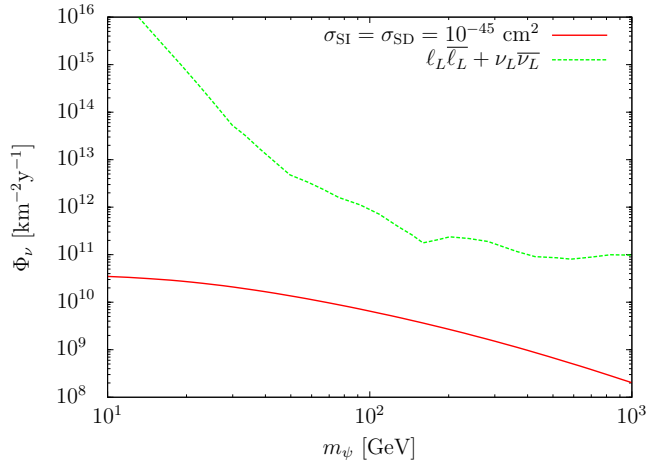


Figure 7: DM mass dependence of total neutrino flux  $\Phi_\nu$ . The expected neutrino flux in the model is given by the red solid line where SI and SD cross sections are fixed to  $\sigma_{\text{SI}} = \sigma_{\text{SD}} = 10^{-45} \text{ cm}^2$ . The upper bound for the channel  $\ell_L\bar{\ell}_L + \nu_L\bar{\nu}_L$  obtained from the IceCube data analysis [66] is given by the green dotted line.

which is far from the canonical annihilation cross section of the thermal DM. The neutrinos from the Sun give a somewhat stronger bound. Monochromatic neutrino emission from DM annihilation has been studied in ref. [68–71]. The differential neutrino flux from the Sun is calculated as

$$\frac{d\Phi_\nu}{dE_\nu} = \frac{1}{2} \frac{C_\odot}{4\pi d^2} \left[ 2\text{Br}(\psi\bar{\psi} \rightarrow \nu\bar{\nu}) \frac{dN_{\nu\bar{\nu}}}{dE_\nu} + \text{Br}(\psi\psi \rightarrow \nu\bar{\psi}) \frac{dN_{\nu\bar{\psi}}}{dE_\nu} \right], \quad (39)$$

where the factor 2 of the first term in Eq. (39) comes from two neutrinos in the final state,  $d = 1.49 \times 10^8 \text{ km}$  is the distance between the Earth and Sun,  $\text{Br}$  is the branching ratio of the process,  $dN_{\nu\bar{\nu}}/dE_\nu$  and  $dN_{\nu\bar{\psi}}/dE_\nu$  are the energy spectra of neutrino for each channel and they are simply written by the delta function in our case. The capture rate in the Sun  $C_\odot$  is estimated by using micrOMEGAs [58]. In particular for  $100 \text{ GeV} \lesssim m_\psi \lesssim 1 \text{ TeV}$ , the capture rate is simply evaluated as

$$C_\odot \approx \left( \frac{1.2 \times 10^{20}}{\text{s}} \right) \left[ \left( \frac{100 \text{ GeV}}{m_\psi} \right)^{1.7} \left( \frac{\sigma_{\text{SI}}}{10^{-45} \text{ cm}^2} \right) + \left( \frac{100 \text{ GeV}}{m_\psi} \right)^{1.9} \left( \frac{\sigma_{\text{SD}}}{10^{-42} \text{ cm}^2} \right) \right], \quad (40)$$

where the Maxwell-Boltzmann distribution is assumed for the DM velocity distribution function with the dispersion  $v_0 = 270 \text{ km/s}$  and the local DM density  $\rho_\odot = 0.3 \text{ GeV/cm}^3$ . The total neutrino flux is simply calculated as

$$\Phi_\nu = \frac{1}{2} \frac{C_\odot}{4\pi d^2} \left( 2\text{Br}(\psi\bar{\psi} \rightarrow \nu\bar{\nu}) + \text{Br}(\psi\psi \rightarrow \nu\bar{\psi}) \right) [\text{km}^{-2}\text{y}^{-1}]. \quad (41)$$

The DM mass dependence of the total neutrino flux is shown in Fig. 7 where both  $\sigma_{\text{SI}}$  and  $\sigma_{\text{SD}}$  are fixed to  $10^{-45} \text{ cm}^2$ , as we evaluated for the large Yukawa parameter sets, and the

sum of the branching ratios in Eq. (41) is taken as 1. In Fig. 7, the IceCube upper bound for  $\ell_L \bar{\ell}_L + \nu_L \bar{\nu}_L$  annihilation channel is also shown. The IceCube bound is obtained by converting the upper bound on the elastic cross section, which has been calculated from the IceCube data [66]. This bound should be understood as a rough reference limit since the annihilation channel is not exactly the same as with our monochromatic case. One finds that the expected neutrino flux in the model is two orders of magnitude smaller than the upper bound at most. To more thoroughly compare the predicted flux with experiments, the effects of neutrino oscillation and propagation together with experimental details should be taken into account.

For the case of small Yukawa coupling, only a single peak of monochromatic neutrino from the semi-annihilation can be seen. It would be difficult to distinguish this from the monochromatic neutrino from the annihilation of typical  $\mathbb{Z}_2$  symmetric DM.

### 3.2.3 Collider Prospects

Generally, DM with a  $\mathbb{Z}_3$  symmetry will give different collider signatures from  $\mathbb{Z}_2$  DM [72, 73]. While only one DM is generated in the final state from the decay of the  $\mathbb{Z}_2$  mother particle, one or two DM particles are produced in the decay of the  $\mathbb{Z}_3$  charged particle. Therefore in the  $\mathbb{Z}_3$  symmetric model, for instance, if the signals of one DM and two DM in the final state have the same visible particles and the intermediate particles are off-shell, the double-kinematic edge would be seen in the invariant mass distribution of the visible particles as a prospect of  $\mathbb{Z}_3$  DM. In our model, however, such decay channels are not expected.

On the other hand, if the intermediate particles are on-shell, the invariant mass distribution will have a different shape in  $\mathbb{Z}_2$  and  $\mathbb{Z}_3$  symmetric models [72, 73]. Considering the decay channel of  $\mathbb{Z}_3$  charged particle with two visible particles separated by a DM, the invariant mass distribution for two visible particles has a cusp. Since such a cuspy feature cannot be present in the decay of  $\mathbb{Z}_2$  odd particle, it gives one possible way to discriminate between  $\mathbb{Z}_2$  and  $\mathbb{Z}_3$  symmetric models. In our model, we can consider the decay of  $\eta^\pm$  which can be produced in pairs via the Drell-Yan process of  $\gamma$  and  $Z$  exchange or singly produced via  $W^\pm$  exchange at the Large Hadron Collider. A concrete example of above decay channel is  $\eta^+ \rightarrow \mu^+ \psi_2 \rightarrow \mu^+ \bar{\psi} \varphi_H^\dagger \rightarrow \mu^+ \bar{\psi} Z \varphi_L^\dagger$ , where the intermediate particles are all on-shell by assuming the mass hierarchy  $m_{\eta^+} > m_2 > m_H > m_L$  and suitable mass differences. The anti-DM particle  $\bar{\psi}$  produced by the decay of  $\psi_2$  separates  $\mu^+$  and  $Z$ , which gives rise to a cusp in the invariant mass distribution for the  $\mu^+ Z$  system. It is noted that the DM mass in this example has to be smaller than  $\sim 70$  GeV, otherwise the mass difference between  $\eta^+$  and  $\varphi_{H,L}$  becomes inconsistent with the EWPT. For example, taking the following mass spectrum for the decay channel:  $m_{\eta^+} = 300$  GeV,  $m_2 = 290$  GeV,  $m_H = 220$  GeV,  $m_L = 120$  GeV,  $m_\psi = 60$  GeV, the constraints we have taken into account can be satisfied by choosing suitable Yukawa couplings,  $y^\nu, y^L$  and  $y^R$ . Detailed signal and background analysis is necessary to estimate detectability of the



cuspy feature. However, this is beyond the scope of this paper.

### 3.3 Complex Scalar Dark Matter

In this section, we discuss the case of complex scalar DM. A similar kind of  $\mathbb{Z}_3$  scalar DM has been studied in ref. [37, 39]. First of all, we should take into account the severe constraint from direct detection of DM. The complex scalar DM  $\varphi \equiv \varphi_L$  with mass  $m_\varphi \equiv m_L$  has an interaction with the  $Z$  boson, since  $\varphi$  includes a component of  $SU(2)_L$  doublet  $\eta^0$ . Thus, much of the parameter space of the mixing angle is excluded by the direct detection experiments like LUX [61] and XENON100 [74]. Here we investigate how small the mixing should be so as to evade the bound. The contribution to the spin independent elastic cross section with nucleus comes from the  $Z$  boson exchange diagram, which is calculated as

$$\sigma_{\text{SI}}^Z = \frac{G_F^2 m_\varphi^2 m_A^2 \sin^4 \alpha}{2\pi (m_\varphi + m_A)^2} [(A - Z) - Z(1 - 4 \sin^2 \theta_W)]^2, \quad (42)$$

where  $A$  is the mass number of nucleus. The elastic cross section with a proton is most stringently constrained by the LUX experiment. The excluded parameter space in  $m_\varphi - \sin \alpha$  plane is shown in the left panel in Fig. 8. The requirement is roughly  $\sin \alpha \lesssim 0.05$ , and we take  $\sin \alpha = 0.05$  in the following discussion. Note that in the ordinary inert doublet model, the constraint from the  $Z$  boson exchange would be weakened by the existence of the mass splitting between CP even and odd inert scalars.

In addition, the scalar coupling  $\lambda_{\phi\chi}$  is also relevant for direct detection via Higgs boson exchange. The elastic cross section is calculated as

$$\sigma_{\text{SI}}^h = \frac{\lambda_{\phi\chi}^2}{4\pi} \frac{m_N^4}{(m_\varphi + m_N)^2 m_h^4} [(A - Z)C_n + ZC_p]^2, \quad (43)$$

where the coefficients  $C_p \approx C_n \approx 0.29$  are calculated from ref. [75]. The constraint on the coupling  $\lambda_{\phi\chi}$  is shown in the right panel in Fig. 8. From this figure, we see that the coupling strength should be  $\lambda_{\phi\chi} \lesssim 0.007$  so as not to conflict with the LUX result in all the DM mass range. Moreover, DM with mass less than 100 GeV tends to be excluded by the vacuum conditions of Eqs. (3)–(5). Note that the two contributions via  $Z$  boson and Higgs boson exchange should be combined together to do a thorough analysis, the above discussion is sufficient to set a conservative limit.

Regarding annihilations of the scalar DM, there are many standard annihilation and semi-annihilation channels such as  $\varphi\varphi^\dagger \rightarrow f\bar{f}, hh, ZZ, W^+W^-$  and  $\varphi\varphi \rightarrow h\varphi^\dagger, Z\varphi^\dagger, W^+\eta^-$  shown in Fig. 9. Since the mixing angle is strictly constrained in our case, the main component of the scalar DM is  $\chi$ , rather than  $\eta^0$ . In Fig. 10 some plots of the DM mass dependence of the relic density are shown for the parameter values given in Tab. 3. The lower bounds of the DM mass are obtained from the vacuum condition Eq. (5) as  $m_\varphi \gtrsim 49$  GeV for the left panels and  $m_\varphi \gtrsim 87$  GeV for the right panels. In the upper

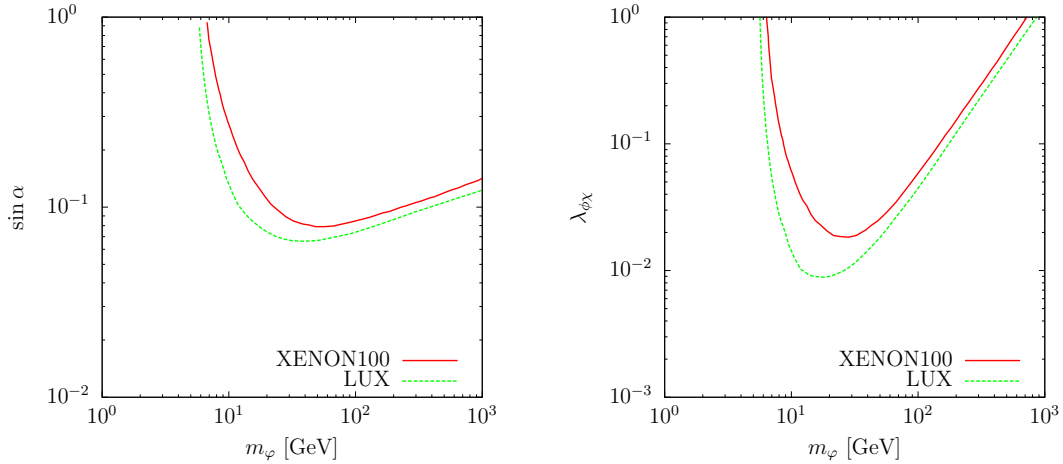


Figure 8: Excluded parameter space in  $m_\varphi - \sin \alpha$  plane (left panel) and  $m_\varphi - \lambda_{\phi\chi}$  (right panel) by XENON100 [74] and LUX [61]. The region above each line is excluded.

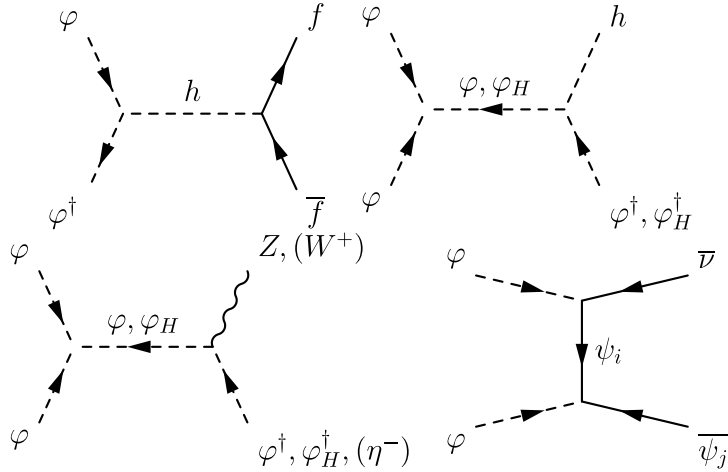


Figure 9: Examples of (semi-)annihilation processes of complex scalar DM  $\varphi$ . For the s-channels written here, the corresponding t-channels also exist.

panels, the region of light DM mass  $12 \text{ GeV} \lesssim m_\varphi \lesssim 30 \text{ GeV}$  is ruled out by the direct detection experiments, while the excluded mass range is  $6 \text{ GeV} \lesssim m_\varphi \lesssim 185 \text{ GeV}$  in the lower panels. In all figures, the relic density of DM is drastically reduced around  $m_\varphi = m_h/2 \approx 63 \text{ GeV}$  due to the annihilation channels  $\varphi\varphi^\dagger \rightarrow h \rightarrow b\bar{b}, W^*W$ . Although the most of the (semi-)annihilations are suppressed for BM-S1 and BM-S2 (upper panels) due to the small  $\lambda_{\phi\chi}$ , the damping around 200 GeV in BM-S1 and 300 GeV in BM-S2 come from the semi-annihilation channels  $\varphi\varphi \rightarrow \varphi_H \rightarrow Z\varphi^\dagger, h\varphi^\dagger$ . These channels are absent in the minimal singlet  $\mathbb{Z}_3$  DM model [39] since there is no second neutral  $\mathbb{Z}_3$  scalar boson. These semi-annihilation channels have a significant contribution when the cubic

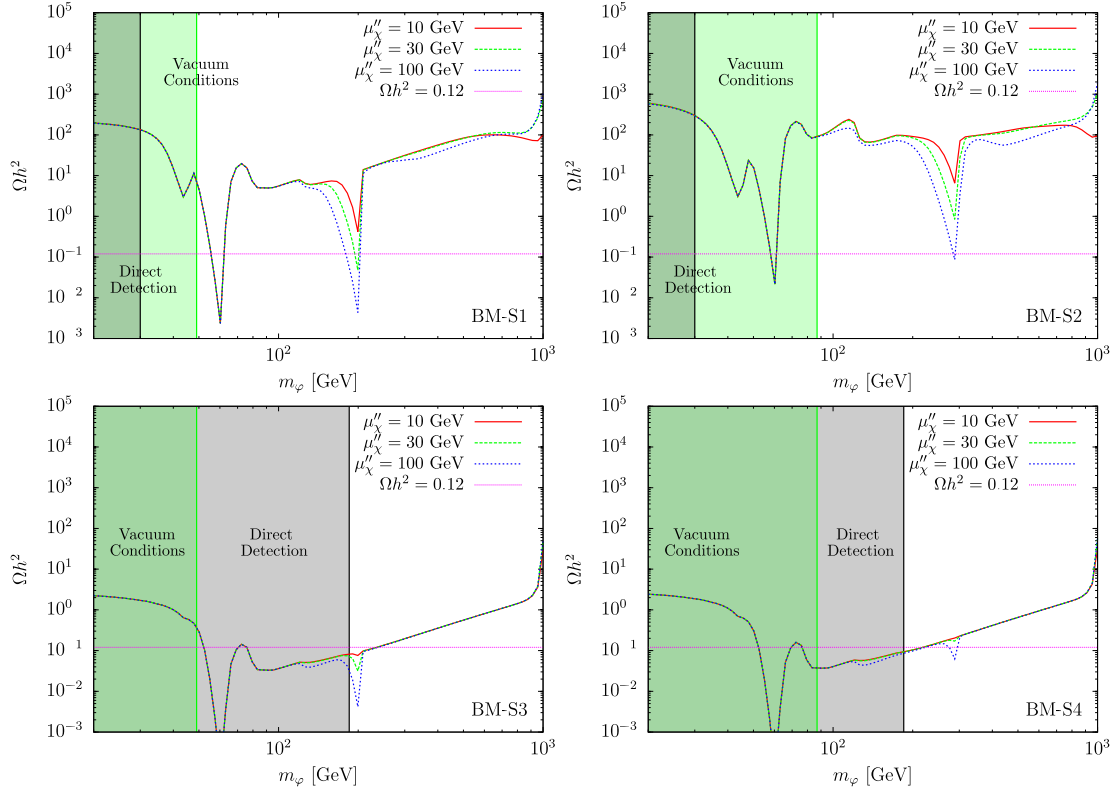


Figure 10: DM mass dependence of relic density where the parameters are taken as in Tab. 3. Note that when one changes  $\mu''_\chi$  as in the figures, the parameters  $y^L$  and  $y^R$  also should be varied from the scale of the neutrino masses.

	$m_H - m_\varphi$ [GeV]	$\lambda_{\phi\chi}$	$\lambda_{\eta\chi}$	$\lambda_2$	$\lambda_3$	$\lambda_4$
BM-S1	200	0.01	1.0	0.1	0.5	0.5
BM-S2	300	0.01	1.0	0.1	0.5	0.5
BM-S3	200	0.1	1.0	0.1	0.5	0.5
BM-S4	300	0.1	1.0	0.1	0.5	0.5

Table 3: Parameter sets of benchmark point for the complex scalar DM. The other parameters are set to  $\sin \alpha = 0.05$ ,  $y_{i\alpha}^\nu = 0.01$ ,  $m_i = 1$  TeV and  $\mu''_\chi(y_{ij}^L + y_{ij}^R) = 10$  GeV.

scalar coupling  $\mu''_\chi$  is large. Another notable point in BM-S1 and BM-S2 is that the relic density of DM is a reduced around  $m_\varphi \approx 1$  TeV for smaller cubic coupling  $\mu''_\chi$  because the co-annihilation  $\varphi\psi_i \rightarrow \bar{\psi}_i \rightarrow \eta^-\bar{\ell}$  is more effective.

For BM-S3 and BM-S4 (lower panels), while the DM mass is strongly constrained by direct detection, the contributions of (semi-)annihilations through the coupling  $\lambda_{\phi\chi}$  can be large and the relic density is much reduced. Thus the  $\mu''_\chi$  dependence becomes relatively smaller than the BM-S1 and BM-S2 cases. Moreover the DM mass scale of several hundred

GeV can be detected by future direct detection experiments like XENON1T.

We have performed an investigation of the case with large Yukawa coupling  $y^\nu$  which is similar to the Dirac DM case. In this case, when  $y^L, y^R \sim \mathcal{O}(1)$  the smaller  $\mu_\chi''$  is required to derive the known neutrino mass scale. As a result, the damping around  $m_\varphi \approx 200$  GeV in BM-S1 and BM-S3 and 300 GeV in BM-S2 and BM-S4 almost disappear. Instead of that, the semi-annihilation channel  $\varphi\varphi \rightarrow \bar{\nu}\bar{\psi}_i$  depicted in the lower right diagram of Fig. 9 affects the DM relic density when the DM is heavier than  $m_\psi/2$ .

As already discussed, although much of the parameter space has already been ruled out by the direct searches for DM, there remains the possibility to detect the complex scalar DM by XENON1T. However, there are essentially no differences from typical  $\mathbb{Z}_2$  symmetric DM. For indirect searches, while the scalar DM basically produces some SM particles such as  $W, Z, h, \ell, \nu$ , it would be difficult to see any characteristic signatures. The annihilation channel  $\varphi^\dagger\varphi \rightarrow \nu\bar{\nu}$  via  $\psi_i$  exchange is suppressed by the small mixing angle  $\sin\alpha$  and it is p-wave suppressed, which is different from the Dirac DM case. Thus even if we assume a large Yukawa coupling  $y^\nu$ , the annihilation cross section is too small to observe, and we have only one monochromatic neutrino emission from the semi-annihilation  $\varphi\varphi \rightarrow \bar{\nu}\bar{\psi}_i$  in the right bottom process in Fig. 9. However, two monochromatic neutrinos would be seen at  $E_\nu = m_\varphi(1 - m_i^2/(4m_\varphi^2))$  from semi-annihilation if the masses of  $\psi_1$  and  $\psi_2$  are different. This process does not exist in the similar  $\mathbb{Z}_3$  scalar DM model of ref. [37].

## 4 Summary and Conclusions

We have considered a model with  $\mathbb{Z}_3$  symmetry. In this model, the neutrino masses are generated at the two-loop level and the known neutrino mass scale has been derived with a reasonable value for the coupling strength. The DM in the model is either a Dirac fermion or a complex scalar as a result of the exact  $\mathbb{Z}_3$  symmetry. The semi-annihilation processes are important to reduce the relic density effectively in the early universe for both of DM particles. We have discussed the DM relic density in the two cases of the small and large Yukawa couplings because of the LFV constraint. In particular for the Dirac DM  $\psi$  with the small Yukawa coupling, although the standard annihilation channel is suppressed, the DM relic density can be compatible with the observed value due to the semi-annihilation processes. Direct detection constrains the complex scalar DM  $\varphi$  to be dominantly singlet. The semi-annihilation processes for the scalar DM are controlled by the cubic coupling  $\mu_\chi''$  and influence the DM relic density.

The  $\mathbb{Z}_3$  symmetric Dirac DM in this model potentially has some interesting signatures, which may be detected by indirect detection and colliders. In particular, for the case with large Yukawa coupling, two monochromatic neutrinos may be observed from the annihilation  $\psi\bar{\psi} \rightarrow \nu\bar{\nu}$  and the semi-annihilation  $\psi\psi \rightarrow \nu\bar{\psi}$  since these cross sections can be the same order of magnitude. The double peak of neutrino flux may be detected

by neutrino observatories such as IceCube. In addition, in the decay of the  $\mathbb{Z}_3$  charged boson  $\eta^+$ , the cusp feature of the invariant mass distribution may be seen at collider experiments. For the complex scalar DM, if the masses of  $\psi_1$  and  $\psi_2$  are different, two monochromatic neutrinos would be emitted from the semi-annihilation  $\varphi\varphi \rightarrow \bar{\nu}\overline{\psi}_i$ .

## Acknowledgments

The authors would like to thank Christopher McCabe for careful reading of the manuscript. The work of M. A. is supported in part by the Grant-in-Aid for Scientific Research, Nos. 25400250 and 26105509. T. T. acknowledges support from the European ITN project (FP7-PEOPLE-2011-ITN, PITN-GA-2011-289442-INVISIBLES). T. T. thanks Kanazawa University for the travel support and local hospitality during some parts of this work.

## References

- [1] M. C. Gonzalez-Garcia, M. Maltoni, J. Salvado and T. Schwetz, JHEP **1212**, 123 (2012) [[arXiv:1209.3023](#) [hep-ph]].
- [2] P. Minkowski, Phys. Lett. B **67**, 421 (1977).
- [3] T. Yanagida, Conf. Proc. C **7902131**, 95 (1979).
- [4] M. Gell-Mann, P. Ramond and R. Slansky, Conf. Proc. C **790927**, 315 (1979) [[arXiv:1306.4669](#) [hep-th]].
- [5] K. G. Begeman, A. H. Broeils and R. H. Sanders, Mon. Not. Roy. Astron. Soc. **249**, 523 (1991).
- [6] P. A. R. Ade *et al.* [Planck Collaboration], [arXiv:1303.5076](#) [astro-ph.CO].
- [7] D. Clowe, M. Bradac, A. H. Gonzalez, M. Markevitch, S. W. Randall, C. Jones and D. Zaritsky, Astrophys. J. **648**, L109 (2006) [[astro-ph/0608407](#)].
- [8] A. Zee, Nucl. Phys. B **264**, 99 (1986).
- [9] K. S. Babu, Phys. Lett. B **203**, 132 (1988).
- [10] L. M. Krauss, S. Nasri and M. Trodden, Phys. Rev. D **67**, 085002 (2003) [[arXiv:hep-ph/0210389](#)].
- [11] E. Ma, Phys. Rev. D **73**, 077301 (2006) [[arXiv:hep-ph/0601225](#)].
- [12] M. Aoki, S. Kanemura and O. Seto, Phys. Rev. Lett. **102**, 051805 (2009) [[arXiv:0807.0361](#)].
- [13] J. March-Russell, C. McCabe and M. McCullough, JHEP **1003**, 108 (2010) [[arXiv:0911.4489](#) [hep-ph]].

- [14] M. Aoki, S. Kanemura, T. Shindou and K. Yagyu, JHEP **1007**, 084 (2010) [Erratum-ibid. **1011**, 049 (2010)] [[arXiv:1005.5159](#)].
- [15] S. Kanemura, O. Seto and T. Shimomura, Phys. Rev. D **84**, 016004 (2011) [[arXiv:1101.5713](#) [hep-ph]].
- [16] S. Kanemura, T. Nabeshima and H. Sugiyama, Phys. Rev. D **85**, 033004 (2012) [[arXiv:1111.0599](#) [hep-ph]].
- [17] M. Gustafsson, J. M. No and M. A. Rivera, Phys. Rev. Lett. **110**, no. 21, 211802 (2013) [[arXiv:1212.4806](#) [hep-ph]].
- [18] D. Hehn and A. Ibarra, Phys. Lett. B **718**, 988 (2013) [[arXiv:1208.3162](#) [hep-ph]].
- [19] P. S. B. Dev and A. Pilaftsis, Phys. Rev. D **86**, 113001 (2012) [[arXiv:1209.4051](#) [hep-ph]].
- [20] P. S. Bhupal Dev and A. Pilaftsis, Phys. Rev. D **87**, no. 5, 053007 (2013) [[arXiv:1212.3808](#) [hep-ph]].
- [21] M. Aoki, J. Kubo and H. Takano, Phys. Rev. D **87**, no. 11, 116001 (2013) [[arXiv:1302.3936](#) [hep-ph]].
- [22] Y. Kajiyama, H. Okada and K. Yagyu, Nucl. Phys. B **874**, 198 (2013) [[arXiv:1303.3463](#) [hep-ph]].
- [23] Y. Kajiyama, H. Okada and T. Toma, Phys. Rev. D **88**, no. 1, 015029 (2013) [[arXiv:1303.7356](#)].
- [24] S. Kanemura, T. Matsui and H. Sugiyama, Phys. Lett. B **727**, 151 (2013) [[arXiv:1305.4521](#) [hep-ph]].
- [25] S. S. C. Law and K. L. McDonald, JHEP **1309**, 092 (2013) [[arXiv:1305.6467](#) [hep-ph]].
- [26] M. Hirsch, R. A. Lineros, S. Morisi, J. Palacio, N. Rojas and J. W. F. Valle, JHEP **1310**, 149 (2013) [[arXiv:1307.8134](#) [hep-ph]].
- [27] D. Restrepo, O. Zapata and C. E. Yaguna, JHEP **1311**, 011 (2013) [[arXiv:1308.3655](#) [hep-ph]].
- [28] M. Lindner, D. Schmidt and A. Watanabe, Phys. Rev. D **89**, 013007 (2014) [[arXiv:1310.6582](#) [hep-ph]].
- [29] H. Okada and K. Yagyu, Phys. Rev. D **89**, 053008 (2014) [[arXiv:1311.4360](#) [hep-ph]].
- [30] S. Baek, H. Okada and T. Toma, [arXiv:1312.3761](#) [hep-ph].
- [31] S. Baek, H. Okada and T. Toma, Phys. Lett. B **732**, 85 (2014) [[arXiv:1401.6921](#) [hep-ph]].
- [32] A. Ahriche, C. -S. Chen, K. L. McDonald and S. Nasri, [arXiv:1404.2696](#) [hep-ph].
- [33] A. Ahriche, K. L. McDonald and S. Nasri, [arXiv:1404.5917](#) [hep-ph].

- [34] S. Kanemura, T. Matsui and H. Sugiyama, [arXiv:1405.1935](#) [hep-ph].
- [35] H. Okada and K. Yagyu, [arXiv:1405.2368](#) [hep-ph].
- [36] F. D’Eramo and J. Thaler, JHEP **1006**, 109 (2010) [[arXiv:1003.5912](#) [hep-ph]].
- [37] G. Belanger, K. Kannike, A. Pukhov and M. Raidal, JCAP **1204**, 010 (2012) [[arXiv:1202.2962](#) [hep-ph]].
- [38] F. D’Eramo, M. McCullough and J. Thaler, JCAP **1304**, 030 (2013) [[arXiv:1210.7817](#) [hep-ph]].
- [39] G. Belanger, K. Kannike, A. Pukhov and M. Raidal, JCAP **1301**, 022 (2013) [[arXiv:1211.1014](#) [hep-ph]].
- [40] P. Ko and Y. Tang, [arXiv:1402.6449](#) [hep-ph].
- [41] G. Blanger, K. Kannike, A. Pukhov and M. Raidal, [arXiv:1403.4960](#) [hep-ph].
- [42] T. Hambye, JHEP **0901**, 028 (2009) [[arXiv:0811.0172](#) [hep-ph]].
- [43] C. Arina, T. Hambye, A. Ibarra and C. Weniger, JCAP **1003**, 024 (2010) [[arXiv:0912.4496](#) [hep-ph]].
- [44] V. V. Khoze, C. McCabe and G. Ro, [arXiv:1403.4953](#) [hep-ph].
- [45] C. Boehm, M. J. Dolan and C. McCabe, Phys. Rev. D **90**, 023531 (2014) [[arXiv:1404.4977](#) [hep-ph]].
- [46] I. P. Ivanov and V. Keus, Phys. Rev. D **86**, 016004 (2012) [[arXiv:1203.3426](#) [hep-ph]].
- [47] M. Aoki, M. Duerr, J. Kubo and H. Takano, Phys. Rev. D **86**, 076015 (2012) [[arXiv:1207.3318](#) [hep-ph]].
- [48] E. Ma, Phys. Lett. B **662**, 49 (2008) [[arXiv:0708.3371](#) [hep-ph]].
- [49] E. Ma and M. Raidal, Phys. Rev. Lett. **87**, 011802 (2001) [Erratum-ibid. **87**, 159901 (2001)] [[hep-ph/0102255](#)].
- [50] J. Adam *et al.* [MEG Collaboration], Phys. Rev. Lett. **110**, no. 20, 201801 (2013) [[arXiv:1303.0754](#) [hep-ex]].
- [51] A. M. Baldini, F. Cei, C. Cerri, S. Dussoni, L. Galli, M. Grassi, D. Nicolo and F. Raffaelli *et al.*, [arXiv:1301.7225](#) [physics.ins-det].
- [52] M. Aoki, S. Kanemura and K. Yagyu, Phys. Rev. D **83**, 075016 (2011) [[arXiv:1102.3412](#) [hep-ph]].
- [53] T. Toma and A. Vicente, JHEP **1401**, 160 (2014) [[arXiv:1312.2840](#) [hep-ph]].
- [54] R. Barbieri, L. J. Hall and V. S. Rychkov, Phys. Rev. D **74**, 015007 (2006) [[hep-ph/0603188](#)].
- [55] M. Baak, M. Goebel, J. Haller, A. Hoecker, D. Kennedy, R. Kogler, K. Moenig and M. Schott *et al.*, Eur. Phys. J. C **72**, 2205 (2012) [[arXiv:1209.2716](#) [hep-ph]].

- [56] A. Semenov, *Comput. Phys. Commun.* **180**, 431 (2009) [[arXiv:0805.0555](#) [hep-ph]].
- [57] A. Alloul, N. D. Christensen, C. Degrande, C. Duhr and B. Fuks, [arXiv:1310.1921](#) [hep-ph].
- [58] G. Belanger, F. Boudjema, A. Pukhov and A. Semenov, *Comput. Phys. Commun.* **185**, 960 (2014) [[arXiv:1305.0237](#) [hep-ph]].
- [59] D. Suematsu, T. Toma and T. Yoshida, *Phys. Rev. D* **79**, 093004 (2009) [[arXiv:0903.0287](#) [hep-ph]].
- [60] D. Schmidt, T. Schwetz and T. Toma, *Phys. Rev. D* **85**, 073009 (2012) [[arXiv:1201.0906](#) [hep-ph]].
- [61] D. S. Akerib *et al.* [LUX Collaboration], [arXiv:1310.8214](#) [astro-ph.CO].
- [62] E. Aprile [XENON1T Collaboration], [arXiv:1206.6288](#) [astro-ph.IM].
- [63] E. Behnke *et al.* [COUPP Collaboration], *Phys. Rev. D* **86**, 052001 (2012) [[arXiv:1204.3094](#) [astro-ph.CO]].
- [64] M. Felizardo, T. A. Girard, T. Morlat, A. C. Fernandes, A. R. Ramos, J. G. Marques, A. Kling and J. Puibasset *et al.*, *Phys. Rev. Lett.* **108**, 201302 (2012) [[arXiv:1106.3014](#) [astro-ph.CO]].
- [65] M. G. Aartsen *et al.* [IceCube Collaboration], *Phys. Rev. Lett.* **110**, 131302 (2013) [[arXiv:1212.4097](#) [astro-ph.HE]].
- [66] A. Ibarra, M. Totzauer and S. Wild, [arXiv:1402.4375](#) [hep-ph].
- [67] R. Abbasi *et al.* [IceCube Collaboration], [arXiv:1210.3557](#) [hep-ex].
- [68] V. D. Barger, W. -Y. Keung and G. Shaughnessy, *Phys. Lett. B* **664**, 190 (2008) [[arXiv:0709.3301](#) [astro-ph]].
- [69] C. Delaunay, P. J. Fox and G. Perez, *JHEP* **0905**, 099 (2009) [[arXiv:0812.3331](#) [hep-ph]].
- [70] S. Andreas, M. H. G. Tytgat and Q. Swillens, *JCAP* **0904**, 004 (2009) [[arXiv:0901.1750](#) [hep-ph]].
- [71] Y. Farzan, *JHEP* **1202**, 091 (2012) [[arXiv:1111.1063](#) [hep-ph]].
- [72] K. Agashe, D. Kim, M. Toharia and D. G. E. Walker, *Phys. Rev. D* **82**, 015007 (2010) [[arXiv:1003.0899](#) [hep-ph]].
- [73] K. Agashe, D. Kim, D. G. E. Walker and L. Zhu, *Phys. Rev. D* **84**, 055020 (2011) [[arXiv:1012.4460](#) [hep-ph]].
- [74] E. Aprile *et al.* [XENON100 Collaboration], *Phys. Rev. Lett.* **109**, 181301 (2012) [[arXiv:1207.5988](#) [astro-ph.CO]].
- [75] G. Belanger, F. Boudjema, A. Pukhov and A. Semenov, *Comput. Phys. Commun.* **180**, 747 (2009) [[arXiv:0803.2360](#) [hep-ph]].